

# Investigating drivers of particulate matter pollution over India and the implications for radiative forcing with GEOS-Chem-TOMAS15

Alexandra Karambelas<sup>1,\*</sup>, Arlene M. Fiore<sup>1,2,^</sup>, Daniel M. Westervelt<sup>1,7</sup>, V. Faye McNeill<sup>3</sup>, Cynthia A. Randles<sup>4</sup>, Chandra Venkataraman<sup>5</sup>, Jeffrey R. Pierce<sup>6</sup>, Kelsey R. Bilsback<sup>6</sup>, George P. Milly<sup>1</sup>

<sup>1</sup> Lamont-Doherty Earth Observatory, Columbia University, Palisades, NY USA

\* Now at Northeast States for Coordinated Air Use Management, Boston, MA USA

<sup>2</sup> Department of Earth and Environmental Sciences, Columbia University, New York, NY USA

<sup>^</sup> Now at Department of Earth, Atmospheric and Planetary Sciences, Massachusetts Institute of Technology, Cambridge, MA, USA

<sup>3</sup> Chemical and Environmental Engineering, Columbia University, New York, NY USA

<sup>4</sup> ExxonMobil Technology and Engineering Company, Annandale, NJ USA

<sup>5</sup> Department of Chemical Engineering, Indian Institute of Technology Bombay, Mumbai, India

<sup>6</sup> Department of Atmospheric Science, Colorado State University, Fort Collins, CO USA

<sup>7</sup> NASA Goddard Institute for Space Studies, New York, NY, USA

Corresponding Author: Alexandra Karambelas ([akarambelas@nescaum.org](mailto:akarambelas@nescaum.org))

## Key Points:

- We establish a new high-resolution India domain nested within a global chemistry model with an option for detailed aerosol microphysics
- PM<sub>2.5</sub> pollution episodes over India vary spatially but are commonly dominated by carbonaceous aerosols.
- Increased scattering aerosols during episodes lower top-of-atmosphere direct radiative effect, enhance cooling and reduce surface shortwave

## 30 Abstract

31 Ambient fine particulate matter (PM<sub>2.5</sub>) concentrations in India frequently exceed 100 µg/m<sup>3</sup> during fall  
32 and winter pollution episodes. We use the GEOS-Chem chemical transport model with the TwO-Moment  
33 Aerosol Sectional microphysics scheme with 15 size bins (TOMAS15) to assess PM<sub>2.5</sub> composition and  
34 impacts on radiation and cloud condensation nuclei (CCN) during pollution episodes as compared to the  
35 seasonal (October-December) average. We conduct high resolution (0.25°x0.3125°) nested-domain  
36 simulations over India for short-duration, high-PM<sub>2.5</sub> episodes in fall 2015 and 2017. The simulations  
37 capture the magnitude and spatial patterns of pollution episodes measured by surface monitors  
38 ( $r^2_{\text{PM}_{2.5}}=0.69$ ) although aerosol optical depth is underestimated. During the episodes, near-surface organic  
39 matter (OM), black carbon (BC), and secondary inorganic aerosol concentrations increase from seasonal  
40 averages by up to 36, 7, and 7 µg/m<sup>3</sup>, respectively. Episodic aerosol increases enhance cooling by lowering  
41 the top-of-atmosphere clear-sky direct radiative effect (DRE<sub>TOA</sub>) during the 2015 episode (-6 W/m<sup>2</sup>), with  
42 a smaller impact during the 2017 episode (-1 W/m<sup>2</sup>). Differences in DRE<sub>TOA</sub> reflect larger increases in  
43 scattering aerosols in the column during the 2015 episode (+17 mg/m<sup>2</sup>) than in 2017 (+13 mg/m<sup>2</sup>), while  
44 absorbing aerosol column enhancements are smaller (+3 mg/m<sup>2</sup>) in both years. Changes in shortwave  
45 radiation at the surface (SW<sub>sfc</sub>) are spatially similar to DRE<sub>TOA</sub> and mostly negative during both episodes.  
46 CCN enhancements during these episodes occur across the western Indo-Gangetic Plain, coincident with  
47 higher PM<sub>2.5</sub> concentrations. Changes in DRE<sub>TOA</sub>, SW<sub>sfc</sub>, and CCN during high-PM<sub>2.5</sub> episodes may have  
48 implications for crops, the hydrologic cycle, and surface temperature.

49

## 50 1. Introduction

51 In recent decades, ambient air pollution in India has grown increasingly worse alongside population  
52 growth, economic development, urbanization, and motorization with limited implementation or  
53 enforcement of regulations on air pollutant emissions. One such pollutant, fine particulate matter with  
54 diameters smaller than 2.5 micrometers (PM<sub>2.5</sub>), regularly exceeds India's National Ambient Air Quality  
55 Standard (NAAQS) of 40 µg/m<sup>3</sup> for annual mean PM<sub>2.5</sub>. Fifty-eight percent of districts exhibit PM<sub>2.5</sub>  
56 concentrations greater than the India NAAQS (Chowdhury et al., 2019), and up to 99.9% of the population  
57 lives in areas exceeding the World Health Organization (WHO) annual mean guideline of 10 µg/m<sup>3</sup>.  
58 Anthropogenic source sectors contribute approximately 60% of India's annual average population-  
59 weighted PM<sub>2.5</sub> concentrations (Venkataraman et al., 2018).

60 In addition to its role in air pollution, PM (also referred to as aerosols) affects climate by altering the  
61 energy balance of the planet through its interactions with radiation and clouds. In this way, aerosols exert  
62 a radiative forcing (IPCC, 2013) on climate, which can lead to disruptions in the monsoon (Dave et al.,  
63 2017; Westervelt et al., 2020) and agriculture (Burney & Ramanathan, 2014; Gupta et al., 2017). The  
64 climate impacts from PM depend on composition, size (diameter), and mass, and are thus expected to vary  
65 in space and time as the balance of PM sources, and their overall magnitude, change. For example, strong  
66 seasonal variations in concentrations and composition will affect bulk optical properties as the mix of  
67 black carbon (BC; strongly absorbing) and sulfate (strongly scattering) varies (Bellouin et al., 2016).  
68 Aerosols can affect or modify the direct radiative effect (DRE)—the difference in instantaneous net  
69 (downward - upward) radiative flux at the top of the atmosphere (TOA) induced by the presence of aerosol.  
70 For instance, TOA direct radiative effects of aerosols from the waste combustion sector alone range from  
71 -0.3 to -0.05 W/m<sup>2</sup> over India (Kodros et al., 2016). Aerosols also impact regional and global climate  
72 indirectly through cloud processes (Albrecht, 1989; Twomey, 1977; Rosenfeld et al., 2008), also known  
73 as aerosol indirect effects, which are among the biggest uncertainties in projecting future climate change  
74 (Myhre et al., 2013).

75

76 Major anthropogenic sources of PM in India include residential biomass (Conibear et al., 2018;  
77 Venkataraman et al., 2018), coal-fired power plants (Guttikunda & Jawahar, 2014), waste burning (Kodros  
78 et al., 2016), and anthropogenic dust (Philip et al., 2017), each of which produces a different chemical mix

79 of both particulate, or primary PM, and gaseous emissions leading to secondary PM. For instance, satellite  
80 instruments have detected a 50% increase of sulfur dioxide, a byproduct of coal-fired power plants and  
81 precursor gas to sulfate aerosol, between 2007 and 2017 (C. Li et al., 2017). Particulate pollution in India  
82 exhibits an annual cycle, with highest surface concentrations in winter associated with a shallow planetary  
83 boundary layer and less precipitation and lowest during the monsoon season because of rainout. PM<sub>2.5</sub>  
84 concentrations during fall and wintertime pollution episodes have been recorded in the several hundreds  
85 and even approaching 1000 µg/m<sup>3</sup>. Episodic contributors to local and regional PM<sub>2.5</sub> pollution include  
86 sources such as seasonal agricultural burning (Liu et al., 2018), the national Diwali holiday (Gautam et  
87 al., 2018), and natural sources like windblown dust. Venkataraman and co-authors (2018) find the biggest  
88 contributions from agricultural burning (approximately 18%) are in the states where the emissions occur—  
89 Punjab and Haryana—and also directly downwind in Delhi. Additionally, enhanced aerosol may be  
90 present at different times throughout the year, for instance windblown dust from nearby deserts in March  
91 through May or persistent Indian outflow over the Bay of Bengal year-round (David et al., 2018). With  
92 PM<sub>2.5</sub> concentrations projected to increase in the future due to higher emissions of organic matter and  
93 secondary inorganic aerosols, and enhanced windblown dust under climate change (Pommier et al., 2017;  
94 Venkataraman et al., 2018), it is increasingly important to understand the current PM composition of  
95 scattering and absorbing aerosols for quantifying future changes and their resulting climate implications.

96  
97 Although sectoral impacts to air quality at present and under future scenarios have been investigated in  
98 India (Chowdhury et al., 2018; Schnell et al., 2018; Venkataraman et al., 2018), less attention has been  
99 given to episodic pollution events in India, with almost no focus on a compositional analysis, or the  
100 implications for climate. For example, although wintertime haze events in urban China are largely  
101 composed of secondary aerosols (Huang et al., 2015), including elevated concentrations during the  
102 COVID-19 related shutdowns across China (Huang et al., 2020; Shi & Brasseur, 2020), the extent to which  
103 these findings are transferable to urban India is unclear.

104  
105 Using the GEOS-Chem global model with a nested high-resolution regional simulation over India, we  
106 examine changes in PM<sub>2.5</sub> aerosol microphysics and the associated direct radiative effect (DRE) during 5-  
107 day peak pollution episodes in fall 2015 and 2017 compared to the annual average (2015) and seasonal  
108 average environment (2015 and 2017); an additional episode from 2016 is included in the Supplemental  
109 Information. We use a high-resolution (0.25° x 0.3125°) nested grid over India with the Two-Moment  
110 Aerosol Sectional (TOMAS) aerosol microphysics package (Adams & Seinfeld, 2002; Kodros & Pierce,  
111 2017; Ramnarine et al., 2019) to simulate PM mass and number size distributions, and chemical  
112 composition. We identify variations in PM composition during peak pollution episodes relative to seasonal  
113 and annual mean values. We compare the baseline model simulations with the limited available *in situ*  
114 observations and satellite aerosol optical depth. Finally, with an offline radiative transfer code that  
115 prescribes optical properties based on the PM composition and size bins for TOMAS as simulated in  
116 GEOS-Chem, we assess the aerosol DRE at TOA during seasonal average and episodic pollution levels.  
117 We also evaluate changes in aerosol number and cloud condensation nuclei (CCN) as a proxy for the  
118 impacts of PM on clouds, an indirect climate impact of aerosols. Our findings suggest peak PM pollution  
119 episodes alter local DRE at TOA by up to -6 W/m<sup>2</sup> and enhance CCN by up to 280%.

## 121 2. Model description and simulation methodology

### 122 2.1 Air Quality Modeling

123 We use the GEOS-Chem chemical transport model version 12.0.2  
124 (<https://doi.org/10.5281/zenodo.1455215>) with standard tropospheric chemistry (Bey et al., 2001), with  
125 and without TOMAS aerosol microphysics. We run simulations both at a global 2° x 2.5° domain and  
126 using a newly developed nested domain over India from 0-40 °N and 60-100 °E at 0.25° x 0.3125° (161  
127 by 162 grid cells). This domain also includes Afghanistan, Bangladesh, Bhutan, Nepal, Pakistan, and parts

128 of neighboring countries. This domain was loosely based on prior work at a  $0.5^\circ \times 0.667^\circ$  resolution with  
129 MERRA-2 meteorological fields from Chaliyakunnel et al. (2019). Stratospheric ozone chemistry is  
130 calculated via the Linoz module (McLinden et al., 2000). We use the baseline tropospheric chemistry  
131 ( $\text{NO}_x\text{-O}_x\text{-HC-aerosol-Br}$ ) with the simple secondary organic aerosol scheme (Pai et al., 2020). We use  
132 the global ECLIPSE anthropogenic emission inventory for year 2015 (Stohl et al., 2015) processed  
133 through the Harvard-NASA Emissions Component (HEMCO) (Keller et al., 2014). Landscape fire  
134 emissions, including agricultural fires, for 2015, 2016, and 2017 are from the Global Fire Emissions  
135 Database (GFED, <https://www.globalfiredata.org>) with small fires and seasonal fire count and emissions  
136 updates in the states of Punjab and Haryana (Liu et al., 2019). During the simulation, GFED emissions  
137 are updated at a 3-hourly timescale, and ECLIPSE emissions are scaled monthly from annual total  
138 emissions. Meteorology is from GEOS-FP for 2015-2017 (Lucchesi, 2013). We processed global GEOS-  
139 FP fields from the  $0.25^\circ \times 0.3125^\circ$  global dataset for the nested domain.

140  
141 TOMAS15 simulates prognostic aerosol number and mass size distributions for 7 chemical species  
142 (sulfate, sea salt, dust, hydrophilic and hydrophobic elemental and organic carbon, and aerosol water),  
143 with 15 sections spanning 3 nm to 10  $\mu\text{m}$  in diameter. Particulate pollutant contributions to total  $\text{PM}_{2.5}$  are  
144 simulated by GEOS-Chem with TOMAS15, hereafter GC-TOMAS15, for sulfate, sea salt, BC, organic  
145 matter (OM), and dust, while nitrate and ammonium are from the standard GEOS-Chem “Tropchem,”  
146 hereafter GC-Tropchem. Sulfate concentrations in the bulk scheme will not necessarily match those in the  
147 TOMAS scheme, particularly as aerosol plumes are transported away from sources as the representations  
148 of dry and wet deposition differ in the size-resolved and bulk aerosol schemes. Our use of bulk ammonium  
149 and nitrate distributed across TOMAS size sections may not be consistent with thermodynamic  
150 equilibrium calculations. However, this technique is a compromise between completely neglecting nitrate  
151 in TOMAS versus including a computationally intensive online treatment of size-dependent ammonium  
152 nitrate partitioning. Average contributions from sea salt and dust during episodes are typically very low  
153 in the model across India ( $< 3\%$ ), which is expected considering these episodes fall outside peak  
154 windblown dust seasons, thus we do not include sea salt and dust in our analysis. We quantify modeled  
155 aerosol component contributions at the surface and in the total column to seasonal and episodic mean  
156 concentrations. We calculate seasonal and episodic CCN using aerosol number concentration from GC-  
157 TOMAS15 and Kappa-Kohler theory (Petters & Kreidenweis, 2007). We note that clouds are not directly  
158 modified by aerosols in our simulations as they are prescribed in the model from the GEOS-FP analysis.  
159 An advantage that TOMAS15 provides over the GEOS-Chem bulk aerosol model is the more physically  
160 realistic size-dependent calculation of AOD and related aerosol optical properties. One disadvantage is  
161 that anthropogenic fugitive dust is not included, which may be a large seasonal contributor to  $\text{PM}_{2.5}$  in  
162 India; this dataset is included in the standard GC-Tropchem model simulations (Philip et al., 2017), but to  
163 our knowledge the size distribution has not been evaluated, so fugitive dust is not included in the size-  
164 resolved TOMAS simulations.

165  
166 We conduct one baseline standard tropospheric chemistry simulation without TOMAS15 (i.e. using  
167 Tropchem) globally at coarse horizontal resolution ( $2^\circ \times 2.5^\circ$ ) for the years 2014-2017 to establish  
168 boundary conditions, where 2014 is solely for initialization purposes. We additionally conduct a full year  
169 baseline Tropchem simulation for 2015 with the regional model ( $0.25^\circ \times 0.3125^\circ$  horizontal resolution)  
170 over India. Due to the computational cost of enabling GC-TOMAS15, we simulate 2014-2015 globally at  
171 coarse resolution ( $2^\circ \times 2.5^\circ$ )—again discarding 2014 as initialization—with subsequent global simulations  
172 restricted to August-December for 2016 and 2017 when PM episodes are highest over India, where August  
173 and September are for initialization only. The 2016 and 2017 GC-TOMAS runs are initialized with August  
174 2015 restart files to reduce spin-up time. We rely on these coarse resolution global simulations for our  
175 assessment of climate impacts quantified with the radiative transfer model as we evaluate changes during  
176 episodic enhancements relative to seasonal means.

177  
178  
179  
180  
181  
182  
183  
184  
185  
186  
187  
188  
189  
190  
191  
192  
193  
194  
195  
196  
197  
198  
199  
200  
201  
202  
203  
204  
205  
206  
207  
208  
209  
210  
211  
212  
213  
214  
215  
216  
217  
218  
219  
220  
221  
222  
223  
224  
225

With the GC-TOMAS15 high-resolution regional model, we conduct a series of 5-day simulations (plus a 5-day initialization period from the coarse resolution output) corresponding to peak episodes in PM<sub>2.5</sub> observed at the U.S. Embassy in Delhi: December 5-9 2015, November 1-5 2016, and November 6-10 2017 (Supplemental Figure 1). These episodes are purposely selected to be outside of the Diwali holiday each year, which occurs annually between mid-October and mid-November, as those emissions are not included in the emissions inventory, though the event contributes to air pollution (e.g. Mukherjee et al., 2020). Daily-average anthropogenic organic carbon (OC) emissions are similar between the 2015 October-December average, 2015 episode, and 2017 episode; biomass burning emissions are nearly double the 2015 seasonal average during the 2017 episode but are roughly half during the 2015 episode (Supplemental Figure 2). Because the 2016 and 2017 episodes are similar in aerosol distribution and climate impacts, we compare the December 2015 and November 2017 episodes in the main text and provide a similar analysis of 2016 in the Supplemental Information. Episodes are compared to the October-December seasonal average from their respective year. We evaluate spatial changes in air pollutant abundances, PM<sub>2.5</sub> composition, and metrics for local climate impacts across the Indo-Gangetic Plain as well as the entire sub-continent during the peak pollution events in Delhi compared to seasonal averages.

Model aerosol optical depth (AOD) is calculated offline using GC-TOMAS output and the radiative transfer code described below following Kodros et al., (2016), and includes black and organic carbon, sulfate, nitrate, ammonium, dust, aerosol water, and sea salt. For AOD observations, we use the Dark Target Level 3 (L3 collection 6) atmosphere daily product retrieved from the Moderate Resolution Imaging Spectroradiometer (MODIS) instrument aboard the Terra and Aqua satellites. This 1° x 1° gridded product is obtained via NASA's Giovanni data portal. The Dark Target MODIS retrieval compares better than Deep Blue versus both the ground-based AERONET AOD over South Asia and the higher-resolution MAIAC retrieval (see Figure 8 of Mhawish et al., 2019).

## 2.2 Radiative transfer model

We use the Rapid Radiative Transfer Model for Global Climate Models (RRTMG) offline and adapted for use with GEOS-Chem TOMAS by Colorado State University (Bilsback et al., 2020a; Bilsback et al., 2020b). Briefly, we use RRTMG to estimate the DRE, or the instantaneous radiative impact at TOA due to episodic aerosol enhancement under clear sky conditions relative to the seasonal average during the selected PM<sub>2.5</sub> pollution episodes, using our 2° x 2.5° GC-TOMAS15 simulations (as we only have the 5-day episodes available from the high-resolution GC-TOMAS15 simulations). We use November solar parameters and three-year GEOS-FP modeled meteorological conditions seasonal averages for the 2015-2017 October-December time frame. We only change the aerosol fields ingested by RRTMG, which include hydrophilic and hydrophobic BC, organic carbon, sulfate, nitrate, ammonium, dust, sea salt, and aerosol water during the specified time period (i.e., episode or seasonal). Note that aerosol water was calculated in all GEOS-Chem simulations according to time-varying relative humidity in the GEOS-FP input meteorology. We also evaluate the change in solar radiation reaching the surface, which has implications for crop growth and the hydrologic cycle.

In calculating DRE, we consider two limiting aerosol mixing states: either fully external or core-shell internal. If external, organic carbon and BC form separate spherical particles. If internal, a BC core is surrounded by other species in a homogeneously mixed shell (Jacobson, 2001). Our DRE estimates thus provides bounds, where core-shell internal mixing serves as a warmer (more positive) forcing and the external mixture a cooler (more negative) forcing. Aerosol number concentration and size distributions are equal across both mixing states. We calculate the change in DRE during the episode from the seasonal mean as:

226  $\Delta DRE_{TOA} = (SW_{TOA\ down} - SW_{TOA\ up})_{episode} - (SW_{TOA\ down} - SW_{TOA\ up})_{seasonal\ mean}$  (1)  
227

228 such that  $DRE_{TOA}$  is a negative quantity for both episode and seasonal mean. Since  $SW_{TOA\ down}$  does not  
229 change between episode and seasonal mean in RRTMG, this equation in effect translates to the change in  
230  $SW$  reflected upwards, such that a decrease in  $DRE_{TOA}$  indicates an increase in  $SW$  reflected upwards  
231 during the episode (i.e. a relative radiative cooling impact). For calculating the change in  $SW$  at the  
232 surface, the parallel equation is:

233  
234  $\Delta SW_{sfc} = (SW_{sfc\ down} - SW_{sfc\ up})_{episode} - (SW_{sfc\ down} - SW_{sfc\ up})_{seasonal\ mean}$  (2)  
235

### 236 3. Evaluating modeled PM<sub>2.5</sub> concentrations

237 We evaluate the baseline simulations with annual and episodic average *in situ* observations of total PM<sub>2.5</sub>  
238 from the Central Pollution Control Board (CPCB) in India as well as satellite observations of aerosol  
239 optical depth (AOD) in the visible wavelength (~550 nm). Observations of PM<sub>2.5</sub> are sparse in India, and  
240 for the December 5-9, 2015 episode, we find 18 sites with hourly observations available for model  
241 evaluation located in northern and central India. Data were collected via the CPCB web portal  
242 (<https://app.cpcbccr.com/ccr/#/caaqm-dashboard-all/caaqm-landing/data>). The average high-resolution  
243 modeled PM<sub>2.5</sub> concentrations for the December 5-9, 2015 episode from the baseline nested India  
244 Tropchem (Figure 1a) simulation are on average 28% lower than from GC-TOMAS15 (Figure 1b).  
245 Distributions between GC-Tropchem and GC-TOMAS are not expected to be identical for inorganic  
246 aerosol, BC, and OM even if emissions were all the same because of size-dependent atmospheric  
247 chemistry, wet removal, and dry deposition relative to the bulk aerosol scheme (Supplemental Figure 3).  
248 Spatial correlations between episode average simulated and all available observed concentrations are  
249 strong (Table 1;  $r^2_{Tropchem\ high-res}=0.69$  and  $r^2_{TOMAS15\ high-res}=0.67$ ), suggesting that both model configurations  
250 capture spatial PM<sub>2.5</sub> concentration gradients across India. At all available monitoring locations, average  
251 observed PM<sub>2.5</sub> concentrations during the pollution episode are 142  $\mu\text{g}/\text{m}^3$ ; high-resolution GC-  
252 TOMAS15 episode average concentrations are 125  $\mu\text{g}/\text{m}^3$  and GC-Tropchem concentrations are lower at  
253 95  $\mu\text{g}/\text{m}^3$ . At measurement sites that exhibited elevated PM<sub>2.5</sub> during the time period (e.g. change in  
254 episodic PM<sub>2.5</sub> from seasonal average > 0), the average observed concentration was 190  $\mu\text{g}/\text{m}^3$  or 34%  
255 higher than the nationwide observed average. Average modeled concentrations are lower than observed  
256 during this time period, and neither GC-TOMAS (excess average at monitors 84  $\mu\text{g}/\text{m}^3$  or +4% higher  
257 than episodic average) nor GC-Tropchem (67  $\mu\text{g}/\text{m}^3$  or +5%) at the coarse resolution can fully replicate  
258 these excess concentrations. Chemical transport models are known to underestimate peak fine PM<sub>2.5</sub>  
259 events in Asia (e.g. Wang et al., 2014), and both coarse resolution model configurations are biased low  
260 against annual average observations (at monitor locations by up to 62  $\mu\text{g}/\text{m}^3$ , Supplemental Figure 4 and  
261 Supplemental Table 1). All evaluation metrics (spatial correlations, temporal correlations, and biases  
262 against observations) improve during periods of pollution episodes like in December 2015 at both coarse-  
263 and high- resolution simulations (Table 1; Supplemental Table 1). As expected, higher resolution  
264 simulations produce a wider range in concentrations, as well as larger enhancements in PM<sub>2.5</sub> during the  
265 episode relative to the seasonal average (Supplemental Figure 5). Although each model configuration has  
266 its own set of strengths and weaknesses as discussed above, we find that overall the high-resolution  
267 simulations with TOMAS fall closest to the observations during the high-pollution episodes on which we  
268 focus our study.

269  
270 Retrievals of AOD from MODIS suggest the nested GC-TOMAS15 underestimates total column AOD  
271 during the pollution events when modeled concentrations are highest (Figure 2; MODIS measurements  
272 aboard Aqua are similar to those from Terra and are shown along with comparisons for the November  
273 2016 episode in Supplemental Figure 6). Modeled AOD, sampled at satellite overpass time, is biased low  
274 for both episodes, during which the model simulates only about 60% of the MODIS AOD, reflecting an

275 unknown combination of underestimated column burdens (including aerosol water uptake) and/or poorly  
276 represented optical properties. Model AOD shows some skill over east India and Bangladesh compared  
277 to satellite retrievals during the 2015 episode, which may be related to aerosol composition during this  
278 particular episode as discussed below.

279  
280 While the simulated AOD here is significantly lower than the MODIS Dark Target product, David et al.  
281 (2018) have previously shown that during the months in which our episodes occur, their modeled AOD  
282 falls between the much lower MISR product and the L2 Collection 6 MODIS product which uses the Deep  
283 Blue retrieval over land and the Dark Target retrieval over oceans. Mhawish et al. (2019), however, show  
284 that the Deep Blue retrieval underestimates the AOD retrieved from AERONET and from the higher  
285 resolution MAIAC product retrieved from MODIS over South Asia. Hence, there is uncertainty in the  
286 observed AOD as well as in the model. Finally, some of our low model bias may be attributable to the  
287 lack of emissions of anthropogenic fugitive dust (Philip et al., 2017) or domestic waste burning including  
288 trash (Wiedinmyer et al., 2014) in GC-TOMAS15, which contribute considerably to annual total PM  
289 emissions, although the extent to which these sectors contribute to pollution episodes is unknown. The  
290 AOD (and surface PM<sub>2.5</sub>) could be further improved in TOMAS15 by the incorporation of size-resolved  
291 sources of anthropogenic fugitive dust (Philip et al., 2017; Xia et al., 2022) and domestic trash (and other  
292 waste) burning (Wiedinmyer et al., 2014), though an overestimate in wet removal resulting from excessive  
293 light rain (Wang et al. 2021) could explain the common underestimate in both GEOS-Chem configurations  
294 that we use here. Mindful of these model biases, we turn next to examine the influence of episodic  
295 enhancements on aerosol concentration and composition and direct and indirect climate impacts.

#### 296 297 **4. Surface PM<sub>2.5</sub> and compositional changes during peak pollution episodes**

298 During the December 5-9 2015 episode, PM<sub>2.5</sub> concentrations in the high-resolution domain average 36  
299  $\mu\text{g}/\text{m}^3$  nationwide but exceed 190  $\mu\text{g}/\text{m}^3$  in Delhi and in the eastern states of Bihar and West Bengal  
300 (Figure 3a). By subtracting episodic total PM<sub>2.5</sub> or component contributions from the seasonal average  
301 using the global coarse resolution configuration with which we simulate the seasonal average, it is possible  
302 to quantify the “excess” PM<sub>2.5</sub> during the pollution episodes. Regions of positive PM<sub>2.5</sub> enhancement are  
303 separated from negative changes by the green contours in Figures 3, 4, 6, and 7. Excess PM<sub>2.5</sub> in the  
304 December 2015 episode is centered over the eastern IGP where concentration enhancements compared to  
305 the 2015 October-to-December mean exceed 50  $\mu\text{g}/\text{m}^3$  (Figure 3b). For comparison, the episodic average  
306 concentration from the coarse GC-TOMAS simulation is also shown (Figure 3c). Episodic concentrations  
307 increase by 15% on average in India, with increases up to 30% in eastern India. Some decreases of 4-6  
308  $\mu\text{g}/\text{m}^3$  occur over western India. Episodic contributions of BC, OM, and the combined sulfate, nitrate, and  
309 ammonium (hereafter referred to as secondary inorganics) follow a similar spatial distribution as the total  
310 concentration enhancement from the seasonal average, with elevated concentrations over Northwest India,  
311 Delhi, and across the eastern IGP. During the 2015 episode, OM is the component with the largest absolute  
312 enhancements, with large swaths of 10-15  $\mu\text{g}/\text{m}^3$  excess OM across the IGP (Figure 3e). Enhancements  
313 are smaller for BC (<4  $\mu\text{g}/\text{m}^3$  Figure 3d). Secondary inorganics increase by 5-7  $\mu\text{g}/\text{m}^3$ , but these  
314 enhancements are more localized to eastern India (Figure 3f) than for the carbonaceous aerosols.

315  
316 During the November 6-10 2017 episode, PM<sub>2.5</sub> concentrations average 32  $\mu\text{g}/\text{m}^3$  nationwide but reach  
317 171  $\mu\text{g}/\text{m}^3$  in Delhi, with elevated concentrations stretching across the IGP (Figure 4a), similar to the 2015  
318 episode. PM<sub>2.5</sub> concentration enhancements during the 2017 episode from the October-December 2017  
319 seasonal average, however, are largest in northwest India over Punjab, Delhi, and into western Uttar  
320 Pradesh (Figure 4b), with enhancements generally between 10 and 30  $\mu\text{g}/\text{m}^3$  and a maximum enhancement  
321 of 52  $\mu\text{g}/\text{m}^3$ . Decreases of 5-20  $\mu\text{g}/\text{m}^3$  relative to the seasonal average occur over eastern and central India  
322 during the 2017 episode, in contrast to the 2015 episode (compare Figures 3b and 4b). During the 2017  
323 episode, changes in BC concentrations relative to the October to December average are small, between -

324  $2 \mu\text{g}/\text{m}^3$  and  $+6 \mu\text{g}/\text{m}^3$  (Figure 4d). Changes in OM are larger, with decreases in the eastern IGP of  $9$   
325  $\mu\text{g}/\text{m}^3$  and increases in the western IGP up to  $36 \mu\text{g}/\text{m}^3$  (Figure 4e). Secondary inorganic aerosol broadly  
326 decreases by  $4\text{--}6 \mu\text{g}/\text{m}^3$  from the seasonal average across much of eastern India during the episode, but  
327 increases over western Uttar Pradesh, Delhi, Punjab, and Haryana by up to  $6 \mu\text{g}/\text{m}^3$  (Figure 4f). The  
328 November 1-5 2016 episode shows similar spatial distributions in episodic average total  $\text{PM}_{2.5}$  and  
329 enhancement of  $\text{PM}_{2.5}$  and components as the 2017 episode (Supplemental Figure 7).

330

331 Our model analysis indicates that these three pollution episodes in India are driven by increases in BC,  
332 OM, and secondary inorganic aerosols, with OM contributing the largest changes (Figures 3 and 4,  
333 Supplemental Figure 7). In regions of positive  $\text{PM}_{2.5}$  enhancements from the October to December  
334 seasonal mean, the episodic changes in these three  $\text{PM}_{2.5}$  components relative to the seasonal mean vary.  
335 At the surface during the 2015 episode, OM, BC, and secondary inorganic aerosols increase on average  
336 by  $4.7 \mu\text{g}/\text{m}^3$ ,  $1.2 \mu\text{g}/\text{m}^3$ , and  $1.1 \mu\text{g}/\text{m}^3$ , respectively. The average magnitude increases in these  
337 components during the 2017 episode are similar ( $+6.0 \mu\text{g}/\text{m}^3$  for OM,  $+1.4 \mu\text{g}/\text{m}^3$  for BC,  $+0.8 \mu\text{g}/\text{m}^3$  for  
338 secondary inorganic aerosols).

339

### 340 **5. Implications of pollution episodes for local energy balances**

341 Aloft, there are major differences between the 2015 and 2017 episode, especially above the boundary  
342 layer (Figure 5). During the 2015 episode, BC, OM, and secondary inorganic concentrations increase  
343 above the boundary layer by 200-300% from the seasonal average, while during the 2017 episode there  
344 are more moderate increases of 50-100% in the mid-troposphere and a corresponding increase in  
345 secondary inorganic aerosols by up to 60% in the lower troposphere (Figure 5). The vertical profile of  
346 aerosols in the 2016 episode shows a lower overall enhancement and similar distribution to the 2017  
347 episode (Supplemental Figure 8).

348

349 Total column enhancements from the October to December seasonal average for BC, OM, and secondary  
350 inorganic aerosol show spatial similarities to the surface  $\text{PM}_{2.5}$  enhancements for the 2015 episode  
351 (compare Figure 6a-c with Figure 3). Strong, isolated column increases of BC (Figure 6a), OM (Figure  
352 6b), and secondary inorganic aerosols (Figure 6c) occur over eastern India and Bangladesh, while the OM  
353 enhancements are larger in magnitude ( $> 30 \text{ mg}/\text{m}^2$ ) and relatively more widespread. Using aerosol fields  
354 archived from GC-TOMAS15, we calculate the change in clear-sky DRE for both external (Figures 6d;  
355 7d) and core-shell (Supplemental Figure 9) mixing assumptions with the offline RRTMG model and find  
356 little quantitative difference in DRE or surface shortwave ( $<1 \text{ W}/\text{m}^2$ ) between these two bounding  
357 assumptions. During the December 5-9 2015 episode, enhanced aerosol scattering leads to a  $6 \text{ W}/\text{m}^2$   
358 decrease in  $\text{DRE}_{\text{TOA}}$  over the eastern states of Bihar, Jharkhand, and West Bengal, and over Bangladesh  
359 (Figure 6d). A negative sign in DRE at TOA indicates a relative cooling tendency and more shortwave  
360 radiation reflected out of the atmosphere by aerosols during the episode as compared to seasonal mean  
361 conditions. Similarly, there is a widespread reduction in the amount of shortwave (SW) radiation (up to  
362  $15 \text{ W}/\text{m}^2$ ) reaching the surface (Figure 6e).

363

364 During the November 6-10, 2017 episode, aerosol column burden enhancements occur over northwestern  
365 India including the states of Punjab and Haryana, Delhi, and western Uttar Pradesh (Figure 7a-c). Over  
366 this region, the OM aerosol burden enhancement compared to seasonal average is between 20 and 30  
367  $\text{mg}/\text{m}^2$  (Figure 7b), while BC (Figure 7a) and secondary inorganic aerosol (Figure 7c) enhancements are  
368 less than  $10 \text{ mg}/\text{m}^2$ . Despite increased aerosol concentrations over northwest India,  $\text{DRE}_{\text{TOA}}$  decreases by  
369 only  $0.5\text{--}1.5 \text{ W}/\text{m}^2$  on average in this region (Figure 7d). During the 2017 episode,  $\text{DRE}_{\text{TOA}}$  increases up  
370 to  $2 \text{ W}/\text{m}^2$  over southern and eastern India compared to the October to December average, indicating a  
371 decrease in backscattered radiation that aligns spatially with the decrease in scattering aerosol (OM and

372 secondary inorganic). Surface SW exhibits broad decreases of up to  $9 \text{ W/m}^2$  over much of northwestern  
373 India and strong increases of over  $4 \text{ W/m}^2$  where there is decreased aerosol at the surface (Figure 7e).

374

375 Changes in the contributions of each component to the column aerosol enhancement vary spatially by  
376 episode and by altitude. Despite similar surface-level magnitude enhancements in regions where peak  
377 levels of aerosols occur during the two episodes, the changes in  $\text{DRE}_{\text{TOA}}$  differ, reflecting different column  
378 burden changes and vertical distributions (Figure 5). We investigate the cause of this difference by  
379 comparing the enhancements in scattering (the sum of secondary inorganics and OM) and absorbing (BC)  
380 aerosols over the regions where the column aerosol burden is enhanced (Figures 6a-c and 7a-c). During  
381 both episodes, BC column burdens increases on average by about  $+3 \text{ mg m}^{-2}$ , but scattering aerosols  
382 increase more during the 2015 episode ( $+17 \text{ mg m}^{-2}$ ) than in 2017 ( $+13 \text{ mg m}^{-2}$ ), with notable differences  
383 in the vertical distribution of the changes between the two episodes shown in Figure 5. More scattering  
384 aerosol mass in the 2015 episode reflects more SW than in the 2017 episode, leading to a larger change in  
385  $\text{DRE}_{\text{TOA}}$  in 2015 than 2017. The scattering aerosol column burden enhancement is even smaller during  
386 2016 ( $+9 \text{ mg m}^{-2}$ ) than in either 2015 or 2017, leading to small changes in  $\text{DRE}_{\text{TOA}}$  relative to the seasonal  
387 average (Supplemental Figure 10, up to  $+2 \text{ W/m}^2$ ). Aerosol mass changes of OM and BC in the regions  
388 where they change are approximately the same between the 2015 and 2017 episodes, suggesting that the  
389 differences in  $\text{DRE}_{\text{TOA}}$  between the two episodes may be due to the different magnitude and directional  
390 changes in sulfate.

391

392 Finally, we examine changes in cloud condensation nuclei (CCN) concentrations to gauge cloud changes  
393 due to aerosol-cloud interactions. Enhancement in episode average CCN (0.2% supersaturation) is most  
394 concentrated over the states of Punjab and Haryana and into Delhi and western Uttar Pradesh, with a  
395 column episodic enhancement of over  $800 \text{ CCN cm}^{-2}$  compared to the October to December average, with  
396 a slightly lower yet still elevated CCN concentration across the IGP for all three pollution episodes  
397 (Figures 6f; 7f; Supplemental 10f). The CCN enhancements are co-located with elevated surface  $\text{PM}_{2.5}$   
398 during episodes (compare Figures 6f, 7f with Figures 3b, 4b) and total aerosol particle number  
399 (Supplemental Figure 11). Although not an exact match, enhanced CCN column burdens often coincide  
400 spatially with increases in surface aerosol concentration more than with column burdens. In regions of  
401  $\text{PM}_{2.5}$  enhancement from the respective year seasonal average, India-total aerosol mass increases of fine  
402 mode (less than  $1 \mu\text{m}$ ) OM, BC, and secondary inorganic aerosols are  $+15\%$ ,  $+24\%$ , and  $+9\%$  for the 2015  
403 episode and  $+17\%$ ,  $+22\%$ , and  $-3\%$  for the 2017 episode. Total (including supermicron sizes) OM, BC,  
404 and secondary inorganic aerosol mass increases from respective seasonal averages are  $+19\%$ ,  $+27\%$ , and  
405  $+12\%$ , respectively, for the 2015 episode and  $+19\%$ ,  $+24\%$ , and  $-2\%$  for the 2017 episode. Increases in  
406 aerosol number and CCN over the western IGP during both episodes may be related to stagnant conditions  
407 conducive to pollution accumulation. Changes in meteorology from the 2015 seasonal mean during the  
408 pollution episodes include shallower planetary boundary layers coincident with regions of excess  $\text{PM}_{2.5}$   
409 during the episodes (Supplemental Figure 12), which could reflect local feedbacks between aerosols and  
410 atmospheric stability (Z. Li et al., 2017; Slater et al., 2022; Wilcox et al., 2016). Cloud cover increases  
411 during the 2015 episode, although decreases occur during the 2016 and 2017 episodes (Supplemental  
412 Figure 12). Wind speeds do not vary significantly between seasonal average and episode, and there is no  
413 clear pattern in relative humidity (not shown).

414

415

## 6. Summary and Discussion

416 In this study, we use two regional and two global configurations of the GEOS-Chem model to determine  
417 changes in total  $\text{PM}_{2.5}$  mass and composition and the response of climate-relevant metrics (direct radiative  
418 effect, CCN, surface shortwave radiation) during peak pollution episodes relative to the overall October  
419 to December pollution season over India. Our newly established regional configuration simulates a high  
420 resolution ( $0.25^\circ \times 0.3125^\circ$ ) domain over India with boundary conditions from the global coarse resolution

421 ( $2^\circ \times 2.5^\circ$ ) GEOS-Chem model. A major advance for evaluating climate metrics such as aerosol-radiation  
422 and aerosol-cloud interactions is the use of the TOMAS aerosol microphysics scheme, which enables an  
423 evaluation of aerosol mass and size distributed across 15 size bins. We simulate air quality using the  
424 standard tropospheric chemistry GEOS-Chem platform (Tropchem) as well as the TOMAS 15-bin aerosol  
425 microphysics scheme (GC-TOMAS15) for the first time with the high-resolution nested India domain for  
426 5-day long enhanced  $PM_{2.5}$  episodes in December 2015 and November 2017 that were identified using  
427 observations at the U.S. Embassy in Delhi (November 2016 episode in the Supplemental Information).  
428 We find that episodic  $PM_{2.5}$  mass concentrations are on average 15% greater than seasonal average  
429 concentrations across the IGP in India, with localized maximum concentration changes upwards of 100%  
430 compared to seasonal average, and reflect combined enhancements in BC, OM, and secondary inorganics.  
431 The absolute changes in OM are larger than the changes in BC and secondary inorganic aerosols, with  
432 little to no contributions from dust and sea salt.

433  
434 We use an offline radiative transfer model (RRTMG) to calculate changes in clear-sky  $DRE_{TOA}$  and  $SW_{sfc}$   
435 during two pollution episodes relative to seasonal mean conditions (October to December). Where  
436 aerosols increase during a pollution episode, clear-sky  $DRE_{TOA}$  is generally negative, implying an overall  
437 cooling influence from the aerosol enhancements. In the December 5-9, 2015 episode, reductions (more  
438 negative) in  $DRE_{TOA}$  (up to  $-6 \text{ W/m}^2$ ) and in  $SW_{sfc}$  (up to  $-15 \text{ W/m}^2$ ) radiation coincide spatially with  
439 enhancements in scattering aerosols (secondary inorganics and OM) and absorbing aerosols (BC) both at  
440 the surface and in the column. Conversely, during the November 6-10, 2017 episode, changes to  $DRE_{TOA}$   
441 are only minimally negative, coincident with increased aerosols (up to  $-1 \text{ W/m}^2$ ) compared to the seasonal  
442 average, yet there are substantial reductions in  $SW_{sfc}$  (up to  $-7 \text{ W/m}^2$ ). We find that the change in clear-  
443 sky  $DRE_{TOA}$  from the October to December average depends on the relative change in scattering versus  
444 absorbing aerosol components. Here we find that there is a larger relative increase in scattering aerosol  
445 column burden during the 2015 episode leading to a stronger negative  $DRE_{TOA}$ , while scattering aerosols  
446 decline slightly in the 2017 episode and lead to virtually no change in  $DRE_{TOA}$ . Our findings suggest that  
447 aerosol and local climate influences are likely to vary with the particular characteristics of a pollution  
448 episode. As expressed in Xia et al. (2022) we expect feedbacks on local meteorology such as suppressed  
449 planetary boundary layer height, which would continue to exacerbate pollution. We also expect the  
450 simulated pollution events to worsen with the addition of missing inventories such as anthropogenic  
451 fugitive dust and trash burning. Additionally, we use aerosol number concentration from TOMAS and  
452 Kappa-Kohler theory to estimate changes in CCN, an indicator of aerosol indirect effect, as a proxy for  
453 episodic impacts on clouds. CCN enhancements are highly concentrated over Delhi during both episodes  
454 and coincident with enhanced inorganic aerosol concentrations during the 2015 episode. Regions of high  
455 CCN resulting from pollution episodes may subsequently influence radiative forcing and cloud cover,  
456 suppressing precipitation (smaller cloud droplets; reduced surface evaporation) and vertical mixing (less  
457 surface shortwave reduces buoyancy), however we did not directly model these feedbacks.

458  
459 From the modeled surface concentrations and contributions, we infer that increased concentrations at the  
460 U.S. embassy in Delhi may signal a broader geographical pollution episode, affecting the length of the  
461 IGP. The pan-Indian pollution problem has been documented previously using air quality models  
462 (Karambelas et al., 2018) and satellite products (Ravishankara et al., 2020). Modeled concentrations in  
463  $PM_{2.5}$  pollution “hot spots” top  $100 \mu\text{g/m}^3$ , although the regions of greatest relative enhancements differ  
464 between episodes, likely reflecting different causes of the pollution episodes. For example, the 2015  
465 wintertime episode may have been triggered by synoptic meteorology favorable for the stagnation of  
466 anthropogenic pollution, while the 2016 and 2017 episodes may be more strongly influenced by seasonal  
467 agricultural fires (e.g. Roozitalab et al., 2020). Aerosol composition is critical to revealing climate  
468 impacts, and the GC-TOMAS15 platform aims to support this understanding. Limitations of this work  
469 include comparing episodes to seasonal average at coarse resolution due to computational constraints, and

470 neglecting brown carbon in the offline radiative transfer code. Further work is needed to understand source  
471 contributions to BC, OM, and secondary organics and the extent to which our findings may generalize  
472 more broadly to other pollution episodes over northern India.

473

#### 474 **Data Availability Statement**

475 Data and code including GEOS-Chem model output, HEMCO diagnostic output, and RRTMG output  
476 calculated by this project and presented in figures and tables are hosted on the Columbia University  
477 Academic Commons at (URL TBD) (Karambelas et al., 2022).

478

#### 479 **Acknowledgements**

480 We acknowledge ExxonMobil Research and Engineering Company for supporting this work. The  
481 GEOS-FP data used in this study/project have been provided by the Global Modeling and Assimilation  
482 Office (GMAO) at NASA Goddard Space Flight Center. We acknowledge Dr. Gus Correa for help with  
483 data archival.

484

#### 485 **Figure Captions**

486 **Figure 1** Average PM<sub>2.5</sub> concentrations during the December 5-9 2015 episode simulated with the  
487 regionally nested high-resolution GEOS-Chem model over India for a) Tropchem and b) GC-TOMAS15  
488 overlaid with observations from the CPCB. The values in the lower left indicate the model area average  
489 (in µg/m<sup>3</sup>) and full range within India

490

491 **Table 1** Model evaluation of PM<sub>2.5</sub> with all available CPCB observations in India averaged over the  
492 October-November-December season or during the December 5-9 2015 pollution episode as shown in  
493 parentheses. Correlations are spatial.

494

495 **Figure 2.** AOD from MODIS Aqua (left column; Dark Target retrieval algorithm) compared with GC-  
496 TOMAS15 1:30 PM local time averaged for each pollution episode (right column) during December 5-9  
497 2015 (top row) and November 6-10 2017 (bottom row).

498

499 **Figure 3** a) Average December 5-9 2015 episode PM<sub>2.5</sub> concentration (0.25 x 0.3125 GC-TOMAS15);  
500 and concentration enhancements during the episode relative to seasonal average for (all 2 x 2.5) b) PM<sub>2.5</sub>  
501 c) average December 5-9 2015 episode PM<sub>2.5</sub> concentrations in the 2 x 2x.5 simulation d) black carbon  
502 (BC) e) organic matter (OM); f) the sum of inorganic aerosols (sulfate, nitrate, and ammonium). A single  
503 contour denoting zero change in total PM<sub>2.5</sub> is superimposed in green.

504

505 **Figure 4** Same as Figure 3 except for the November 6-10 2017 episode.

506

507 **Figure 5** Average concentration differences in the column above regions where the surface PM<sub>2.5</sub>  
508 episodic enhancement is positive, for (a) black carbon, (b) organic matter, and (c) secondary inorganic  
509 aerosol. The red lines are for the relative (%) change of the 2017 episode from the 2017 October to  
510 December average and blue shows the relative (%) change of the 2015 episode from the 2015 October to  
511 December average.

512

513 **Figure 6** Changes in the column burdens of a) black carbon b) organic matter c) secondary inorganics  
514 during the December 5-9, 2015 pollution episode from seasonal average (October-December) in the GC-  
515 TOMAS15 coarse horizontal resolution (global) simulations (seasonal fields are only available at coarse  
516 resolution). Also shown are changes during the episode from the seasonal mean of d) direct radiative effect  
517 (DRE) at the top of the atmosphere (TOA); e) net surface shortwave (SW) radiation; f) total column cloud

518 condensation nuclei (0.2% supersaturation). The singular contour for zero change is shown in green.  
519 Negative DRE and SW are indicative of cooling.  
520  
521 **Figure 7** Same as Figure 6 except for the November 6-10, 2017 episode.  
522

523 **References**

- 524 Adams, P. J., & Seinfeld, J. H. (2002). Predicting global aerosol size distributions in general circulation  
525 models. *Journal of Geophysical Research*, *107*(D19). <https://doi.org/10.1029/2001JD001010>
- 526 Albrecht. (1989). Aerosols, Cloud Microphysics, and Fractional Cloudiness. *Science*, *245*(4923),  
527 3131227–1230. <https://doi.org/10.1126/science.245.4923.1227>
- 528 Bellouin, Nicolas, Baker, L., Hodnebrog, Ø., Olivié, D., Cherian, R., Macintosh, C., et al. (2016). Regional  
529 and seasonal radiative forcing by perturbations to aerosol and ozone precursor emissions.  
530 *Atmospheric Chemistry and Physics*, *16*(21), 13885–13910. [https://doi.org/10.5194/acp-16-](https://doi.org/10.5194/acp-16-13885-2016)  
531 13885-2016
- 532 Bey, I., Jacob, D. J., Yantosca, R. M., Logan, J. A., Field, B. D., Fiore, A. M., et al. (2001). Global modeling  
533 of tropospheric chemistry with assimilated meteorology: Model description and evaluation.  
534 *Journal of Geophysical Research: Atmospheres*, *106*(D19), 23073–23095.  
535 <https://doi.org/10.1029/2001JD000807>
- 536 Biltsback, K. R., Kerry, D., Croft, B., Ford, B., Jathar, S. H., Carter, E., et al. (2020). Beyond SO<sub>x</sub> reductions  
537 from shipping: assessing the impact of NO<sub>x</sub> and carbonaceous-particle controls on human  
538 health and climate. *Environmental Research Letters*, *15*(12), 124046.  
539 <https://doi.org/10.1088/1748-9326/abc718>
- 540 Biltsback, K. R., Baumgartner, J., Cheeseman, M., Ford, B., Kodros, J. K., Li, X., et al. (2020). Estimated  
541 Aerosol Health and Radiative Effects of the Residential Coal Ban in the Beijing-Tianjin-Hebei  
542 Region of China. *Aerosol and Air Quality Research*, *20*(11), 2332–2346.  
543 <https://doi.org/10.4209/aaqr.2019.11.0565>
- 544 Burney, J., & Ramanathan, V. (2014). Recent climate and air pollution impacts on Indian agriculture.  
545 *Proceedings of the National Academy of Sciences*, *111*(46), 16319–16324.  
546 <https://doi.org/10.1073/pnas.1317275111>

547 Chaliyakunnel, S., Millet, D. B., & Chen, X. (2019). Constraining Emissions of Volatile Organic  
548 Compounds Over the Indian Subcontinent Using Space-Based Formaldehyde Measurements.  
549 *Journal of Geophysical Research: Atmospheres*, 124(19), 10525–10545.  
550 <https://doi.org/10.1029/2019JD031262>

551 Chowdhury, S., Dey, S., & Smith, K. R. (2018). Ambient PM<sub>2.5</sub> exposure and expected premature  
552 mortality to 2100 in India under climate change scenarios. *Nature Communications*, 9(1).  
553 <https://doi.org/10.1038/s41467-017-02755-y>

554 Chowdhury, S., Dey, S., Guttikunda, S., Pillarisetti, A., Smith, K. R., & Di Girolamo, L. (2019). Indian  
555 annual ambient air quality standard is achievable by completely mitigating emissions from  
556 household sources. *Proceedings of the National Academy of Sciences*, 116(22), 10711–10716.  
557 <https://doi.org/10.1073/pnas.1900888116>

558 Conibear, L., Butt, E. W., Knote, C., Arnold, S. R., & Spracklen, D. V. (2018). Residential energy use  
559 emissions dominate health impacts from exposure to ambient particulate matter in India.  
560 *Nature Communications*, 9(1). <https://doi.org/10.1038/s41467-018-02986-7>

561 Dave, P., Bhushan, M., & Venkataraman, C. (2017). Aerosols cause intraseasonal short-term  
562 suppression of Indian monsoon rainfall. *Scientific Reports*, 7(1), 17347.  
563 <https://doi.org/10.1038/s41598-017-17599-1>

564 David, L. M., Ravishankara, A. R., Kodros, J. K., Venkataraman, C., Sadavarte, P., Pierce, J. R., et al.  
565 (2018). Aerosol Optical Depth Over India. *Journal of Geophysical Research: Atmospheres*,  
566 123(7), 3688–3703. <https://doi.org/10.1002/2017JD027719>

567 Gautam, S., Yadav, A., Pillarisetti, A., Smith, K., & Arora, N. (2018). Short-Term Introduction of Air  
568 Pollutants from Fireworks During Diwali in Rural Palwal, Haryana, India: A Case Study. *IOP*

569 *Conference Series: Earth and Environmental Science*, 120, 012009.  
570 <https://doi.org/10.1088/1755-1315/120/1/012009>

571 Guenther, A. B., Jiang, X., Heald, C. L., Sakulyanontvittaya, T., Duhl, T., Emmons, L. K., & Wang, X.  
572 (2012). The Model of Emissions of Gases and Aerosols from Nature version 2.1 (MEGAN2.1): an  
573 extended and updated framework for modeling biogenic emissions. *Geoscientific Model*  
574 *Development*, 5(6), 1471–1492. <https://doi.org/10.5194/gmd-5-1471-2012>

575 Gupta, R., Somanathan, E., & Dey, S. (2017). Global warming and local air pollution have reduced  
576 wheat yields in India. *Climatic Change*, 140(3–4), 593–604. [https://doi.org/10.1007/s10584-](https://doi.org/10.1007/s10584-016-1878-8)  
577 [016-1878-8](https://doi.org/10.1007/s10584-016-1878-8)

578 Guttikunda, S. K., & Jawahar, P. (2014). Atmospheric emissions and pollution from the coal-fired  
579 thermal power plants in India. *Atmospheric Environment*, 92, 449–460.  
580 <https://doi.org/10.1016/j.atmosenv.2014.04.057>

581 Huang, R. J., Zhang, Y., Bozzetti, C., Ho, K. F., Cao, J. J., Han, Y., et al. (2015). High secondary aerosol  
582 contribution to particulate pollution during haze events in China. *Nature*, 514(7521), 218–222.  
583 <https://doi.org/10.1038/nature13774>

584 Huang, X., Ding, A., Gao, J., Zheng, B., Zhou, D., Qi, X., et al. (2020). Enhanced secondary pollution  
585 offset reduction of primary emissions during COVID-19 lockdown in China. *National Science*  
586 *Review*, 0, 1–9.

587 IPCC. (2013). *CLIMATE CHANGE 2013 The Physical Science Basis*. Intergovernmental Panel on Climate  
588 Change.

589 Jaeglé, L., Quinn, P. K., Bates, T. S., Alexander, B., & Lin, J.-T. (2011). Global distribution of sea salt  
590 aerosols: new constraints from in situ and remote sensing observations. *Atmospheric Chemistry*  
591 *and Physics*, 11(7), 3137–3157. <https://doi.org/10.5194/acp-11-3137-2011>

592 Karambelas, A., Fiore, A. M., Westervelt, D.M., McNeill, V.F., Randles, C.A., Venkataraman, C., Pierce,  
593 J.R., Bilsback, K.R., Milly, G.P. (2022). Investigating drivers of particulate matter pollution over  
594 India and the implications for radiative forcing with GEOS-Chem-TOMAS15: Data and Code  
595 [Dataset]. Columbia University Academic Commons. URL TBD.

596 Karambelas, A., Holloway, T., Kinney, P. L., Fiore, A. M., DeFries, R., Kieseewetter, G., & Heyes, C. (2018).  
597 Urban versus rural health impacts attributable to PM2.5 and O3 in northern India.  
598 *Environmental Research Letters*, 13(6), 064010. <https://doi.org/10.1088/1748-9326/aac24d>

599 Keller, C. A., Long, M. S., Yantosca, R. M., Da Silva, A. M., Pawson, S., & Jacob, D. J. (2014). HEMCO v1.0:  
600 A versatile, ESMF-compliant component for calculating emissions in atmospheric models.  
601 *Geoscientific Model Development*, 7(4), 1409–1417. <https://doi.org/10.5194/gmd-7-1409-2014>

602 Kodros, J. K., & Pierce, J. R. (2017). Important global and regional differences in aerosol cloud-albedo  
603 effect estimates between simulations with and without prognostic aerosol microphysics:  
604 DIFFERENCES IN CLOUD-ALBEDO AEROSOL INDIRECT EFFECT. *Journal of Geophysical Research:*  
605 *Atmospheres*, 122(7), 4003–4018. <https://doi.org/10.1002/2016JD025886>

606 Kodros, John K., Cucinotta, R., Ridley, D. A., Wiedinmyer, C., & Pierce, J. R. (2016). The aerosol radiative  
607 effects of uncontrolled combustion of domestic waste. *Atmospheric Chemistry and Physics*,  
608 16(11), 6771–6784. <https://doi.org/10.5194/acp-16-6771-2016>

609 Li, C., McLinden, C., Fioletov, V., Krotkov, N., Carn, S., Joiner, J., et al. (2017). India Is Overtaking China  
610 as the World’s Largest Emitter of Anthropogenic Sulfur Dioxide. *Scientific Reports*, 7(1).  
611 <https://doi.org/10.1038/s41598-017-14639-8>

612 Li, Z., Guo, J., Ding, A., Liao, H., Liu, J., Sun, Y., et al. (2017). Aerosol and boundary-layer interactions  
613 and impact on air quality. *National Science Review*, 4(6), 810–833.  
614 <https://doi.org/10.1093/nsr/nwx117>

615 Liang et al. (2010). Finding the missing stratospheric Br<sub>y</sub>: a global modeling study of CHBr<sub>3</sub> and CH<sub>2</sub>Br<sub>2</sub>,  
616 Atmos. Chem. Phys., doi:10.5194/acp-10-2269-2010.

617 Liu, T., Marlier, M. E., DeFries, R. S., Westervelt, D. M., Xia, K. R., Fiore, A. M., et al. (2018). Seasonal  
618 impact of regional outdoor biomass burning on air pollution in three Indian cities: Delhi,  
619 Bengaluru, and Pune. *Atmospheric Environment*, 172(September 2017), 83–92.  
620 <https://doi.org/10.1016/j.atmosenv.2017.10.024>

621 Liu, T., Marlier, M., Karambelas, A., Jain, M., Singh, S., Singh, M., et al. (2019). Missing emissions from  
622 post-monsoon agricultural fires in northwestern India: regional limitations of MODIS burned  
623 area and active fire products. *Environmental Research Communications*, 1(01), 1007.  
624 <https://doi.org/10.31223/osf.io/9jvak>

625 Lucchesi, R. (2013). File Specification for GEOS-5 FP, No. 4(Version 1.0), 63.

626 Marais, E. and C. Wiedinmyer (2016). *Air quality impact of Diffuse and Inefficient Combustion Emissions*  
627 *in Africa (DICE-Africa)*, Environ. Sci. Technol., 50(19), 10739–10745,  
628 doi:10.1021/acs.est.6b02602.

629 McLinden, C. A., Olsen, S. C., Hannegan, B., Wild, O., Prather, M. J., & Sundet, J. (2000). Stratospheric  
630 ozone in 3-D models: A simple chemistry and the cross-tropopause flux. *Journal of Geophysical*  
631 *Research: Atmospheres*, 105(D11), 14653–14665. <https://doi.org/10.1029/2000JD900124>

632 Mhawish, A., Banerjee, T., Sorek-Hamer, M., Lyapustin, A., Broday, D. M., & Chatfield, R. (2019).  
633 Comparison and evaluation of MODIS Multi-angle Implementation of Atmospheric Correction  
634 (MAIAC) aerosol product over South Asia. *Remote Sensing of Environment*, 224, 12–28.  
635 <https://doi.org/10.1016/j.rse.2019.01.033>

636 Mukherjee, T., Vinoj, V., Midya, S. K., Puppala, S. P., & Adhikary, B. (2020). Numerical simulations of  
637 different sectoral contributions to post monsoon pollution over Delhi. *Heliyon*, 6(3), e03548.  
638 <https://doi.org/10.1016/j.heliyon.2020.e03548>

639 Murray, L. T., Jacob, D. J., Logan, J. A., Hudman, R. C., & Koshak, W. J. (2012). Optimized regional and  
640 interannual variability of lightning in a global chemical transport model constrained by LIS/OTD  
641 satellite data: IAV OF LIGHTNING CONSTRAINED BY LIS/OTD. *Journal of Geophysical Research:*  
642 *Atmospheres*, 117(D20). <https://doi.org/10.1029/2012JD017934>

643 Pai, S. J., Heald, C. L., Pierce, J. R., Farina, S. C., Marais, E. A., Jimenez, J. L., et al. (2020). An evaluation  
644 of global organic aerosol schemes using airborne observations. *Atmos. Chem. Phys.*, 29.

645 Petters, M. D., & Kreidenweis, S. M. (2007). A single parameter representation of hygroscopic growth  
646 and cloud condensation nucleus activity. *Atmos. Chem. Phys.*, 11.

647 Philip, S., Martin, R. V., Snider, G., Weagle, C. L., van Donkelaar, A., Brauer, M., et al. (2017).  
648 Anthropogenic fugitive, combustion, and industrial dust is significant, underrepresented fine  
649 particulate matter source in global atmospheric models. *Environmental Research Letters*,  
650 044018. <https://doi.org/10.1088/1748-9326/aa65a4>

651 Pommier, M., Fagerli, H., Gauss, M., Simpson, D., Sharma, S., Sinha, V., et al. (2017). Impact of regional  
652 climate change and future emission scenarios on surface O<sub>3</sub> and PM<sub>2.5</sub> over India. *Atmospheric*  
653 *Chemistry and Physics Discussions*, 185194, 1–41. <https://doi.org/10.5194/acp-2017-519>

654 Ramnarine, E., Kodros, J. K., Hodshire, A. L., Lonsdale, C. R., Alvarado, M. J., & Pierce, J. R. (2019).  
655 Effects of near-source coagulation of biomass burning aerosols on global predictions of aerosol  
656 size distributions and implications for aerosol radiative effects. *Atmospheric Chemistry and*  
657 *Physics*, 19(9), 6561–6577. <https://doi.org/10.5194/acp-19-6561-2019>

658 Ravishankara, A. R., David, L. M., Pierce, J. R., & Venkataraman, C. (2020). Outdoor air pollution in India  
659 is not only an urban problem. *Proceedings of the National Academy of Sciences*, *117*(46),  
660 28640–28644. <https://doi.org/10.1073/pnas.2007236117>

661 Rosenfeld, D., et al. (2008), Flood or drought: How do aerosols affect precipitation?  
662 *Science*, **321**, 1309–1313. <https://doi.org/10.1126/science.1160606>.

663 Roozitalab, B., Carmichael, G. R., & Guttikunda, S. K. (2020). *Improving regional air quality predictions*  
664 *in the Indo-Gangetic Plain-Case study of an intensive pollution episode in November 2017*  
665 (preprint). Aerosols/Atmospheric Modelling/Troposphere/Chemistry (chemical composition  
666 and reactions). <https://doi.org/10.5194/acp-2020-744>

667 Schnell, J. L., Naik, V., Horowitz, L. W., Paulot, F., Mao, J., Ginoux, P., et al. (2018). Exploring the  
668 relationship between surface PM<sub>2.5</sub> and meteorology in Northern India. *Atmospheric Chemistry*  
669 *and Physics*, *18*(14), 10157–10175. <https://doi.org/10.5194/acp-18-10157-2018>

670 Sherwen, T., Schmidt, J. A., Evans, M. J., Carpenter, L. J., Großmann, K., Eastham, S. D., et al. (2016).  
671 Global impacts of tropospheric halogens (Cl, Br, I) on oxidants and composition in GEOS-Chem.  
672 *Atmospheric Chemistry and Physics*, *16*(18), 12239–12271. [https://doi.org/10.5194/acp-16-](https://doi.org/10.5194/acp-16-12239-2016)  
673 [12239-2016](https://doi.org/10.5194/acp-16-12239-2016)

674 Shi, X., & Brasseur, G. P. (2020). The Response in Air Quality to the Reduction of Chinese Economic  
675 Activities During the COVID-19 Outbreak. *Geophysical Research Letters*, *47*(11).  
676 <https://doi.org/10.1029/2020GL088070>

677 Slater, J., Coe, H., McFiggans, G., Tonttila, J., & Romakkaniemi, S. (2022). The effect of BC on aerosol–  
678 boundary layer feedback: potential implications for urban pollution episodes. *Atmospheric*  
679 *Chemistry and Physics*, *22*(4), 2937–2953. <https://doi.org/10.5194/acp-22-2937-2022>

680 Stettler, M. E. J., Eastham, S., & Barrett, S. R. H. (2011). Air quality and public health impacts of UK  
681 airports. Part I: Emissions. *Atmospheric Environment*, 45(31), 5415–5424.  
682 <https://doi.org/10.1016/j.atmosenv.2011.07.012>

683 Stohl, A., Aamaas, B., Amann, M., Baker, L. H., Bellouin, N., Berntsen, T. K., et al. (2015). Evaluating the  
684 climate and air quality impacts of short-lived pollutants. *Atmospheric Chemistry and Physics*,  
685 15(18), 10529–10566. <https://doi.org/10.5194/acp-15-10529-2015>

686 Tzompa-Sosa, Z. A., Mahieu, E., Franco, B., Keller, C. A., Turner, A. J., Helmig, D., et al. (2017). Revisiting  
687 global fossil fuel and biofuel emissions of ethane. *Journal of Geophysical Research:*  
688 *Atmospheres*, 122(4), 2493–2512. <https://doi.org/10.1002/2016JD025767>

689 Twomey, S., The influence of pollution on the short wave albedo of clouds, *J. Atmos. Sci.*, **34**, 1149–  
690 1152, 1977.

691 Van Der Werf, G. R., Randerson, J. T., Giglio, L., Collatz, G. J., Mu, M., Kasibhatla, P. S., et al. (2010).  
692 Global fire emissions and the contribution of deforestation, savanna, forest, agricultural, and  
693 peat fires (1997-2009). *Atmospheric Chemistry and Physics*, 10(23), 11707–11735.  
694 <https://doi.org/10.5194/acp-10-11707-2010>

695 Venkataraman, C., Brauer, M., Tibrewal, K., Sadavarte, P., Ma, Q., Cohen, A., et al. (2018). Source  
696 influence on emission pathways and ambient PM2.5 pollution over India (2015-2050).  
697 *Atmospheric Chemistry and Physics Discussions*, (December), 1–38.  
698 <https://doi.org/10.5194/acp-2017-1114>

699 Vinken, G. C. M., Boersma, K. F., Jacob, D. J., & Meijer, E. W. (2011). Accounting for non-linear  
700 chemistry of ship plumes in the GEOS-Chem global chemistry transport model. *Atmospheric*  
701 *Chemistry and Physics*, 11(22), 11707–11722. <https://doi.org/10.5194/acp-11-11707-2011>

702 Wang, L. T., Wei, Z., Yang, J., Zhang, Y., Zhang, F. F., Su, J., et al. (2014). The 2013 severe haze over  
703 southern Hebei, China: Model evaluation, source apportionment, and policy implications.  
704 *Atmospheric Chemistry and Physics*, *14*(6), 3151–3173. [https://doi.org/10.5194/acp-14-3151-](https://doi.org/10.5194/acp-14-3151-2014)  
705 2014

706 Wang, Y., Xia, W., Liu, X. *et al.* Disproportionate control on aerosol burden by light rain. *Nat.*  
707 *Geosci.* **14**, 72–76 (2021). <https://doi.org/10.1038/s41561-020-00675-z>

708 Westervelt, D. M., You, Y., Li, X., Ting, M., Lee, D. E., & Ming, Y. (2020). Relative Importance of  
709 Greenhouse Gases, Sulfate, Organic Carbon, and Black Carbon Aerosol for South Asian  
710 Monsoon Rainfall Changes. *Geophysical Research Letters*, *47*(13).  
711 <https://doi.org/10.1029/2020GL088363>

712 Wiedinmyer, C., Yokelson, R. J., & Gullett, B. K. (2014). Global Emissions of Trace Gases, Particulate  
713 Matter, and Hazardous Air Pollutants from Open Burning of Domestic Waste. *Environmental*  
714 *Science & Technology*, *48*(16), 9523–9530. <https://doi.org/10.1021/es502250z>

715 Wilcox, E. M., Thomas, R. M., Praveen, P. S., Pistone, K., Bender, F. A.-M., & Ramanathan, V. (2016).  
716 Black carbon solar absorption suppresses turbulence in the atmospheric boundary layer.  
717 *Proceedings of the National Academy of Sciences*, *113*(42), 11794–11799.  
718 <https://doi.org/10.1073/pnas.1525746113>

719 Xia, W., Wang, Y., Chen, S., Huang, J., Wang, B., Zhang, G. J., et al. (2022). Double Trouble of Air  
720 Pollution by Anthropogenic Dust. *Environmental Science & Technology*, *56*(2), 761–769.  
721 <https://doi.org/10.1021/acs.est.1c04779>

722

## Figures and Tables

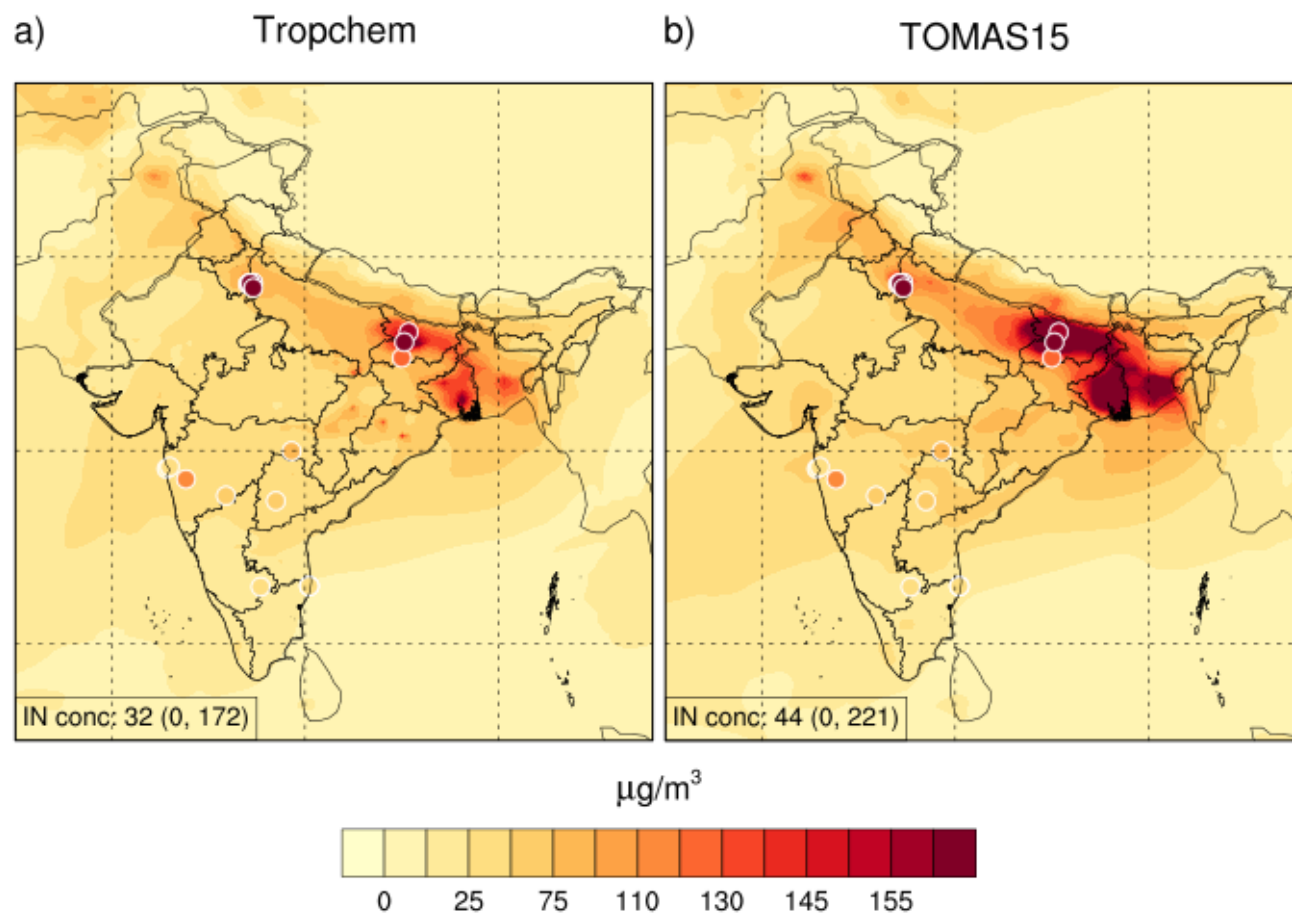


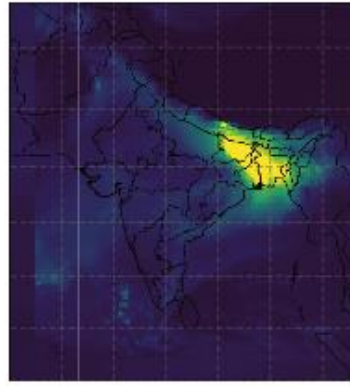
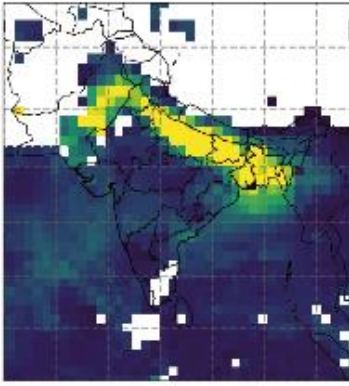
**Figure 1** Average PM<sub>2.5</sub> concentrations during the December 5-9 2015 episode simulated with the regionally nested high-resolution GEOS-Chem model over India for a) Tropchem and b) GC-TOMAS15 overlaid with observations from the CPCB. The values in the lower left indicate the model area average (in µg/m<sup>3</sup>) and full range within India

	Model Average (µg/m <sup>3</sup> )	Observed Average µg/m <sup>3</sup> )	# Points	Mean Fractional Bias	Normalized Mean Bias	Normalized Mean Error	r <sup>2</sup>
<b>Tropchem 2x2.5 (December episode)</b>	47 (64)	144 (142)	22 (18)	-95% (-63%)	-67% (-55%)	67% (56%)	0.60 (0.40)
<b>GC-TOMAS15 2x2.5 (December episode)</b>	58 (80)	144 (142)	22 (18)	-79% (-45%)	-59% (-44%)	60% (47%)	0.59 (0.36)
<b>Tropchem 0.25x0.3125 (December episode)</b>	69 (95)	144 (142)	22 (18)	-71% (-40%)	-52% (-33%)	52% (36%)	0.49 (0.69)
<b>GC-TOMAS15 0.25x0.3125 (December episode only)</b>	(125)	(142)	(18)	(-16%)	(-12%)	(34%)	(0.67)

**Table 1** Model evaluation of PM<sub>2.5</sub> with all available CPCB observations in India averaged over the October-November-December season or during the December 5-9 2015 pollution episode as shown in parentheses. Correlations are spatial.

Dec 5-9 2015, Dark Target (Aqua)

GC 1330IST Dec 5-9 2015



Nov 6-10 2017, Dark Target (Aqua)

GC 1330IST Nov 6-10 2017

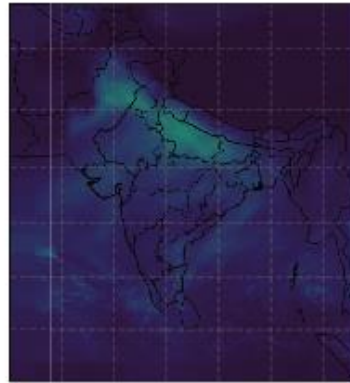
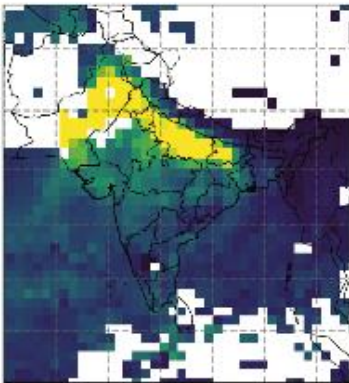


**Figure 2.** AOD from MODIS Aqua (left column; Dark Target retrieval algorithm) compared with GC-TOMAS15 1:30 PM local time averaged for each pollution episode (right column) during December 5-9 2015 (top row) and November 6-10 2017 (bottom row).

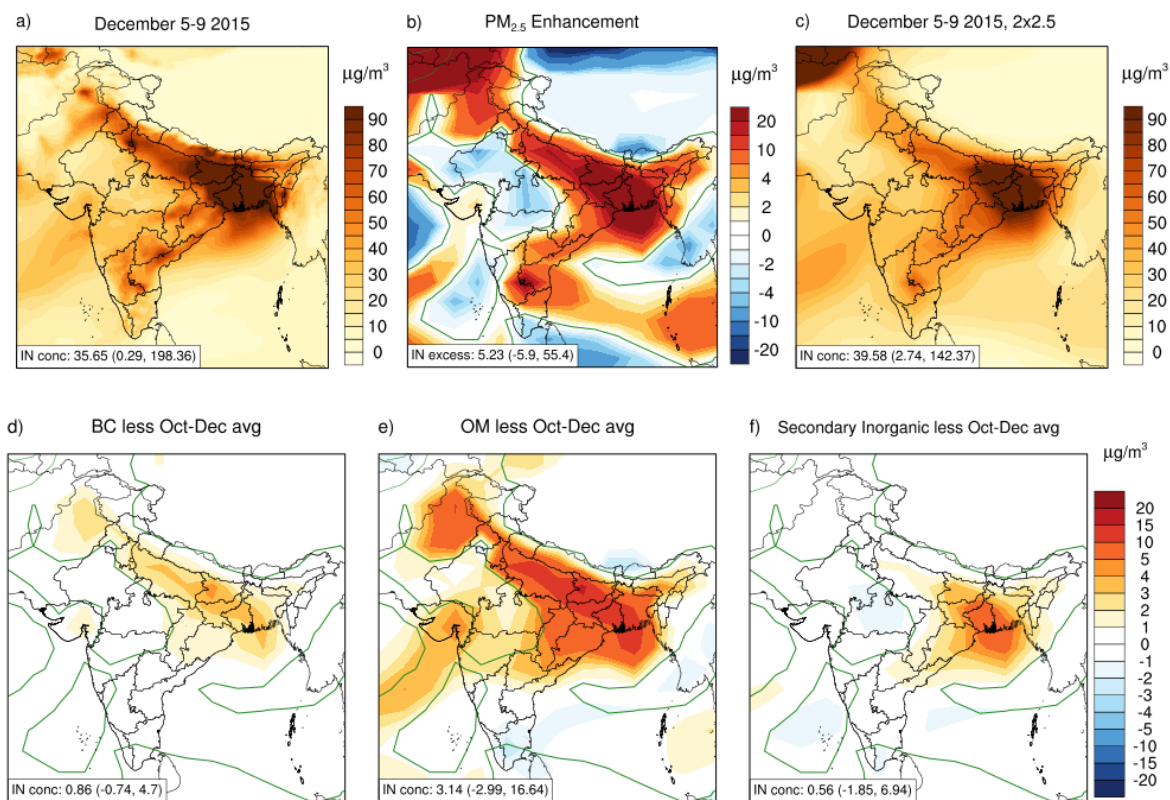


**Figure 3** a) Average December 5-9 2015 episode  $PM_{2.5}$  concentration ( $0.25 \times 0.3125$  GC-TOMAS15); and concentration enhancements during the episode relative to seasonal average for (all  $2 \times 2.5$ ) b)  $PM_{2.5}$  c) average December 5-9 2015 episode  $PM_{2.5}$  concentrations in the  $2 \times 2x.5$  simulation d) black carbon (BC) e) organic matter (OM); f) the sum of inorganic aerosols (sulfate, nitrate, and ammonium). A single contour denoting zero change in total  $PM_{2.5}$  is superimposed in green.

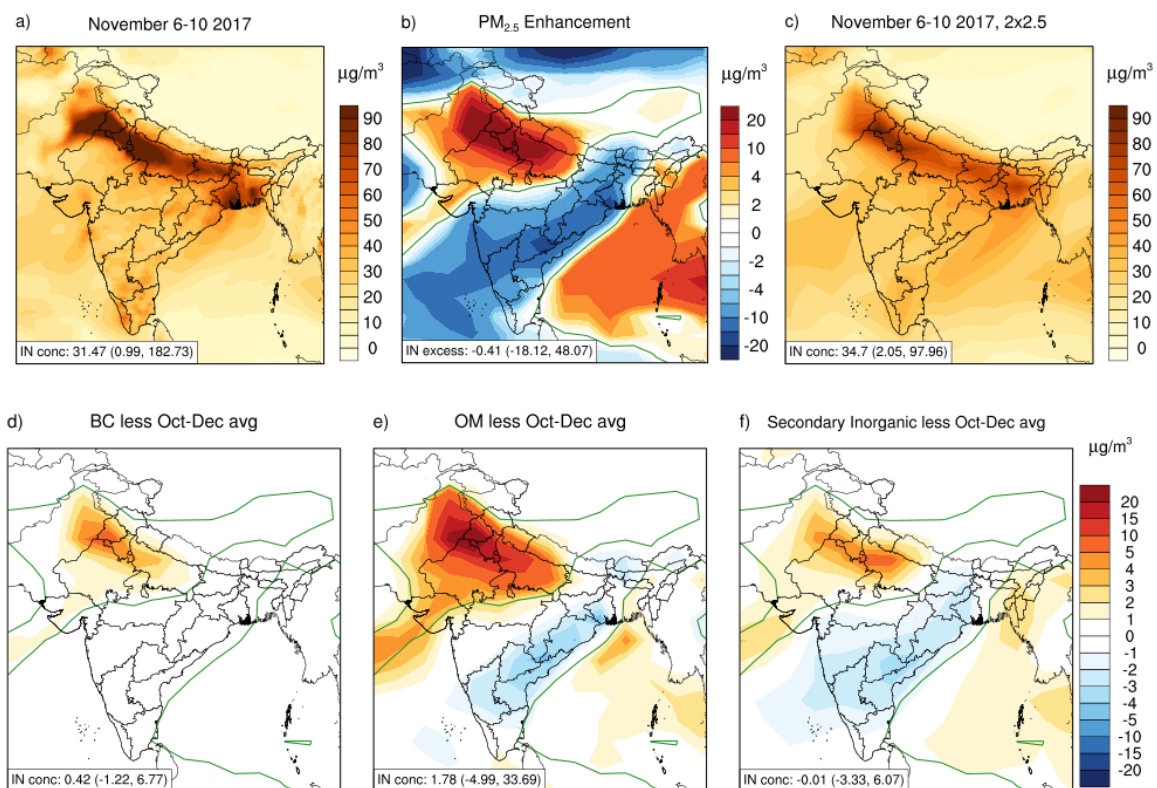


**Figure 4** Same as Figure 3 except for the November 6-10 2017 episode.

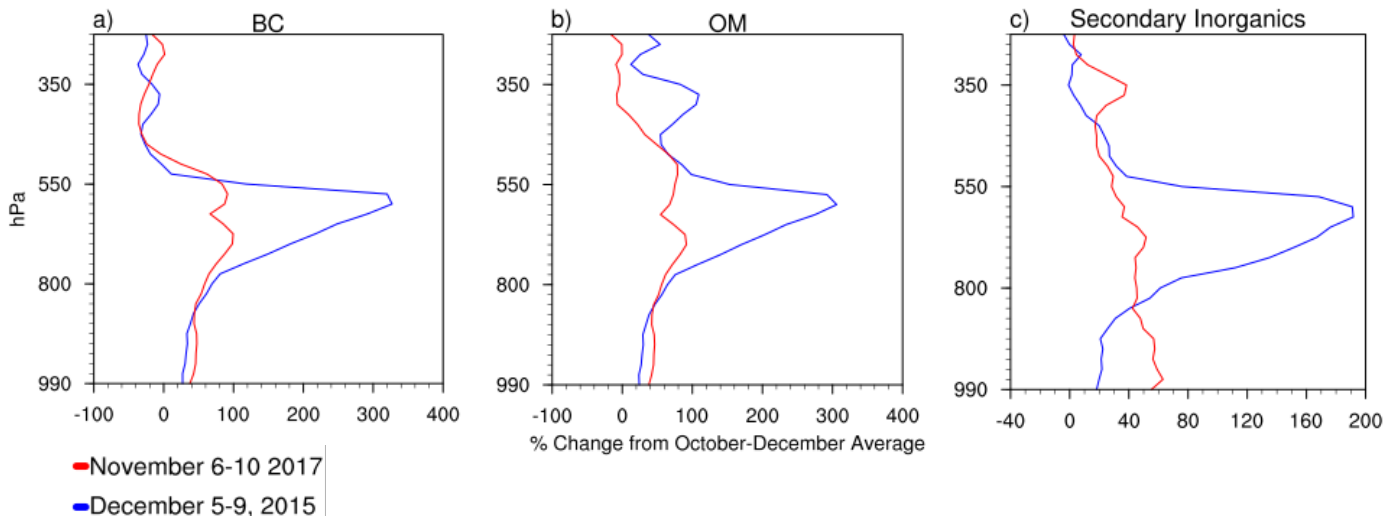


**Figure 5** Average concentration differences in the column above regions where the surface  $PM_{2.5}$  episodic enhancement is positive, for (a) black carbon, (b) organic matter, and (c) secondary inorganic aerosol. The red lines are for the relative (%) change of the 2017 episode from the 2017 October to December average and blue shows the relative (%) change of the 2015 episode from the 2015 October to December average.

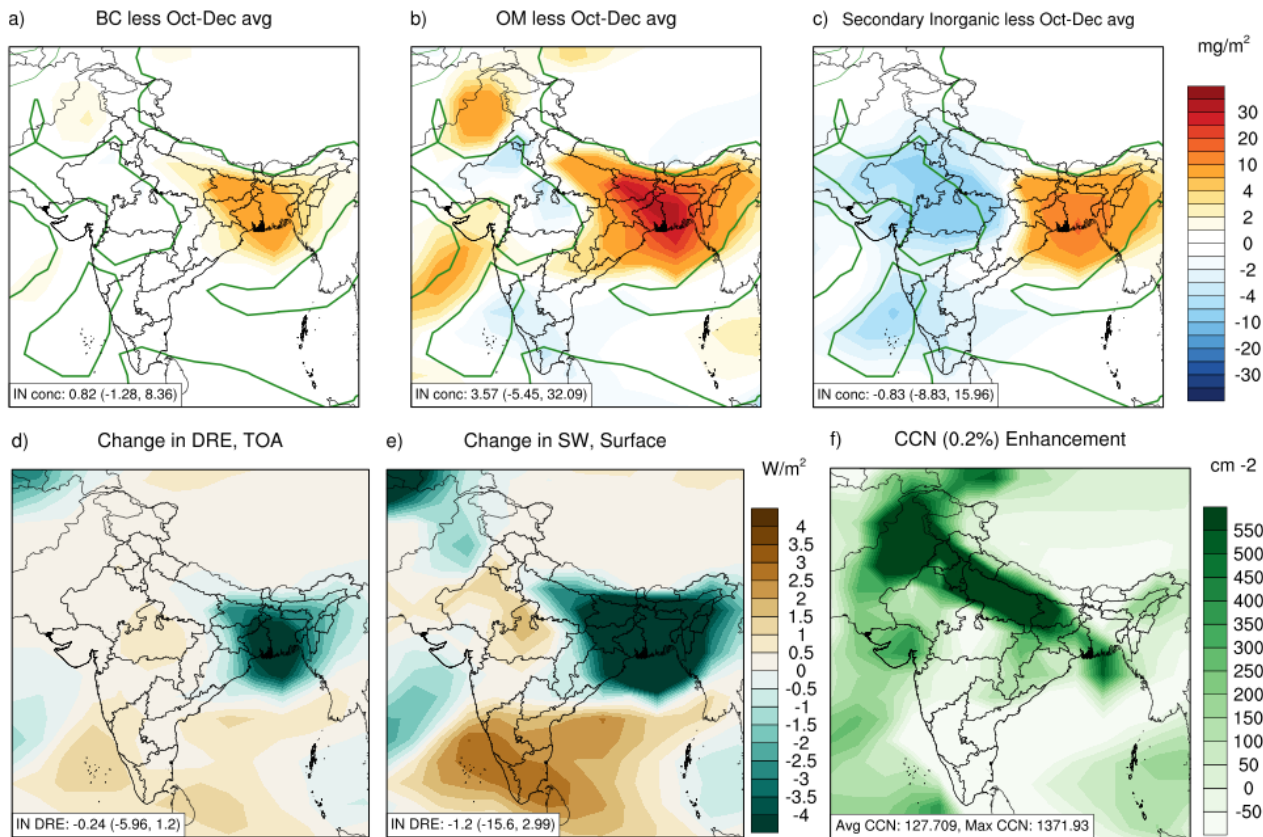


**Figure 6** Changes in the column burdens of a) black carbon b) organic matter c) secondary inorganics during the December 5-9, 2015 pollution episode from seasonal average (October-December) in the GC-TOMAS15 coarse horizontal resolution (global) simulations (seasonal fields are only available at coarse resolution). Also shown are changes during the episode from the seasonal mean of d) direct radiative effect (DRE) at the top of the atmosphere (TOA); e) net surface shortwave (SW) radiation; f) total column cloud condensation nuclei (0.2% supersaturation). The singular contour for zero change is shown in green. Negative DRE and SW are indicative of cooling.

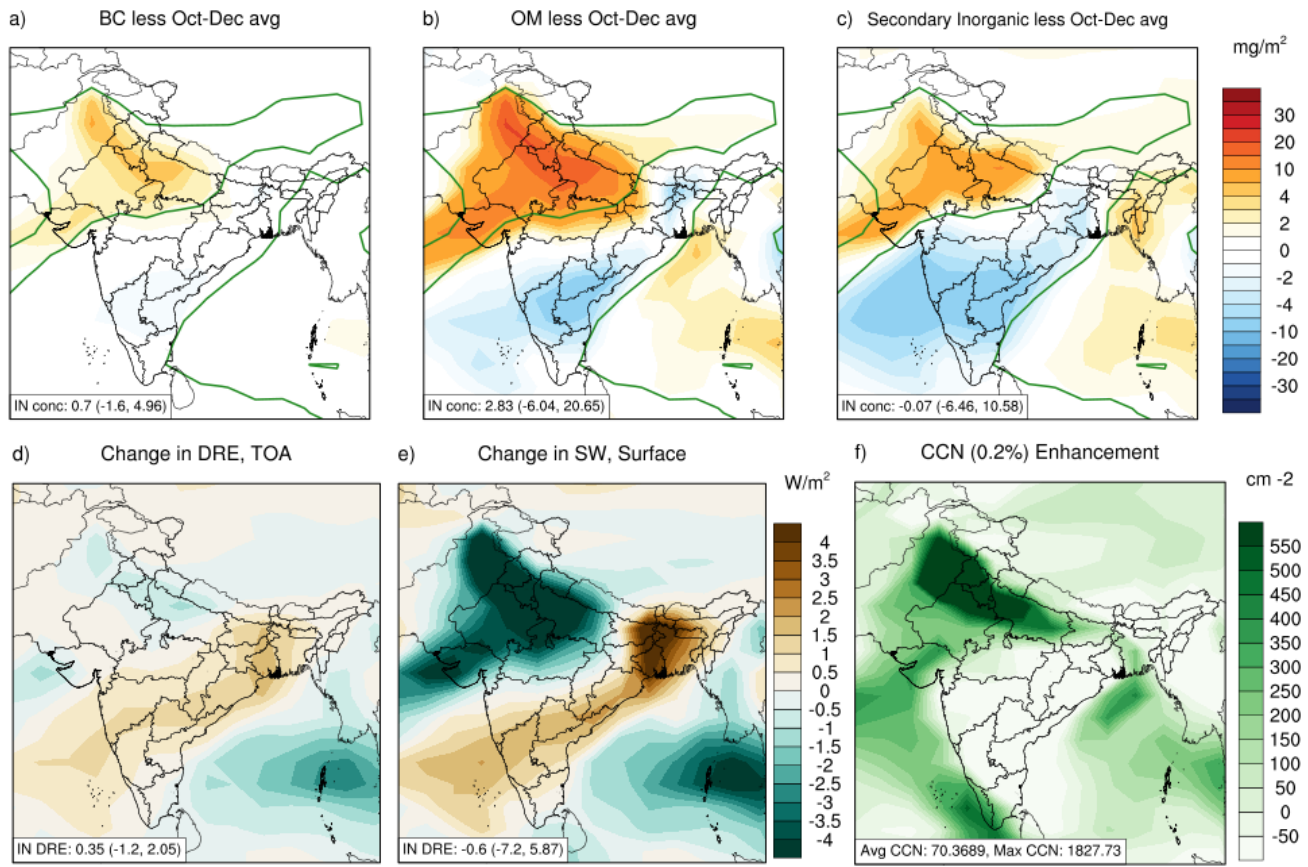


**Figure 7** Same as Figure 6 except for the November 6-10, 2017 episode.